PROCESSING MODULE

The journey from raw data to useful output involves a series of steps which draw from different signal processing algorithmic approaches. A flowchart for the data flow through the software application is visualized in Figure . The data acquired by the software from memory is just the raw data output from the sensor, in the form of a normalized intensity measured by each pixel of the sensor. For one measurement there are eight such pieces of data, representing a frame capture of the light as modified by the cell sample. Each chunk of data represents a slightly shifted image of the cell sample, a product of the moving spatial filter in the design. These chunks can be compared and collimated to produce a single, higher-resolution intensity map through a process known as pixel super-resolution.

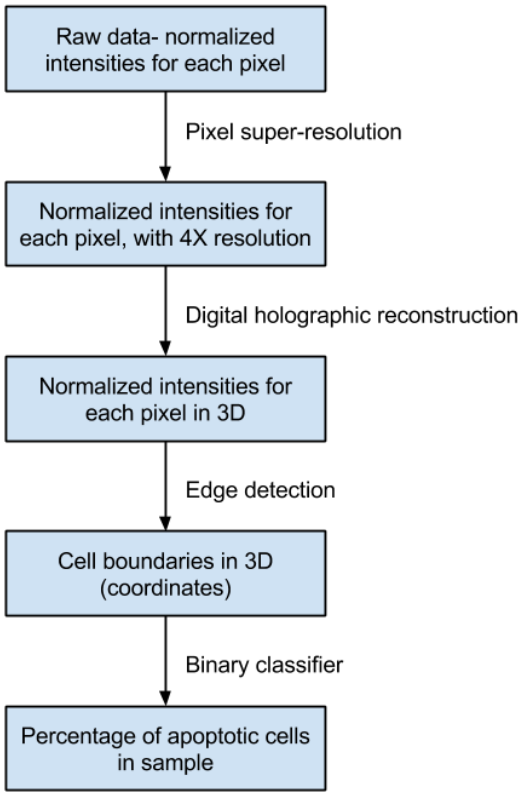

Figure 24: Flowchart of data flow

The super-resolved intensity maps, or images, are then reconstructed as holograms to project the 2D data into 3 dimensions. Finally the apoptotic percentage is calculated by classifying cells based on their membrane (biological) or edge (as sensed in computer vision) morphology. In the following paragraphs we outline the algorithmic approaches for each step along the processing from raw intensity data to apoptotic cell data.

The first step in the processing is to superresolve the raw data. In Bishara et al's implementation of holographic reconstruction of microscopic objects on a chip, the super-resolution technique is similar to the one we plan to implement[i]. For each sample, 8 frames of data are collected under different lighting conditions as potentiated by a motor which moves the pinhole spatial filter a certain distance prior to measurement. The sub-millimeter shifts in peak illumination intensity result in subpixel shifting of the sample with respect to the sensor, allowing for interpolation given a super-resolution algorithm. Essentially the sampling rate of the in tensity data is

increased. The assumption is that each pixel sampled by the sensor is a linear combination of the underlying higher-resolution images. To determine the relative placements of the pixels, a cost function detailing the error between the images is optimized:

$$C(Y) = \frac{1}{2} \sum_{all\ weights\ k,i} \left(x_{k,i} - x'_{k,i}\right)^2 + \frac{\alpha}{2}(Y_P^T * Y_P)$$

where Y is the high resolution image, Y_P is a high pass filter of the image, α is a weight given to high frequencies (may be arbitrary based on results), x is a single pixel from a vector in one image and x' is a single pixel from a vector in another image. A minimization of the cost function yields Y, which is just the planar intensity at high resolution. Comparing the high resolution image to one of the lower resolution images, a mean pixel function can be computed, which when convolved with the high resolution image, will provide additional resolution similar to Gaussian averaging super-resolution[ii].

Reconstruction of the object from its now super-resolved diffraction pattern is based on the Rayleigh-Sommerfeld diffraction formulas. We use an angular spectrum method for reconstruction because of its projected speed in processing. The equation relates the normalized plane wave amplitude, E, in one unit of propagation in the z direction (distance or time, with z direction normal to the object wave) to the wavelength of light, λ, and dimensions of the holography setup[iii,iv]:

$$E_2(x_2, y_2, z) = \int_{-\infty}^{\infty}\int_{-\infty}^{\infty} E_1(x_1, y_1, 0) \cdot \frac{e^{i\frac{2\pi}{\lambda}r_1}}{r_1} \cdot \frac{z}{r_1}\left(\frac{1}{2\pi r_1} + \frac{1}{i\lambda}\right) dx_1 dy_1$$

Where r_1 is the distance from the origin of propagation, in our case the pinhole spatial filter, with x and y normalized and z representing the distance above the focal plane:

$$r_1 = \sqrt{(x_2 - x_1)^2 + (y_2 - y_1)^2 + z^2}$$

A numerical method for this computation is provided by a convolution propagation. A convolution kernel is convolved with the previous angular spectrum value to obtain the next value:

$$E_2 = E_1(x_1, y_1, 0) * h(x, y, z)$$

$$h(x_1, y_1, z) = \frac{e^{i\frac{2\pi}{\lambda}r_1}}{r} \cdot \frac{z}{r} \cdot \left(\frac{1}{2\pi r_1} + \frac{1}{i\lambda}\right)$$

$$r = \sqrt{x_2^2 + y_2^2 + z_2^2}$$

Which is written in Fourier domain as

$$F\{h(x, y, z)\} = \iint h(x, y, z) \cdot e^{-i2\pi(f_x x + f_y y)} dxdy = e^{i2\pi \cdot f_z \cdot z}$$

Where f_x, f_y, and f_z are the Fourier frequencies in the x, y, and z directions. The rightmost equality holds true because the Fourier frequencies are dependent on one another as follows:

$$f_z = \sqrt{\frac{1}{\lambda^2} - f_x^2 - f_y^2}$$

Having established the Fourier transform of the convolution kernel, to reproduce the Fourier transform of the 3D field of light intensity we just multiply with the planar light intensity as measured by the sensor:

$$F\{E(x, y, z)\} = F\{E(x, y, 0)\} \cdot F\{h(x, y, z)\}$$

Finally an inverse Fourier transform brings back the plane wave amplitude. Note that the information coming off of the sensor is a normalized intensity value, which we can easily convert to plane wave amplitude:

$$I_0(r) = |E_0(r)|^2$$

This is the boundary condition as well as a proportionality rule, i.e. the boundary condition is applied at both ends, with intensity as measured by the sensor at the sensing end and intensity as provided by the light source at the sourcing end, and a power fit is applied to reconstruct normalized plane wave from intensity.

After the 3D hologram of the sample has been reproduced, the software must find the cells and measure their surface morphology. Canny detection is a common edge detector in computer vision which provides good detection, localization, minimal response, and little noise[v]. We implement an adaptation of Canny algorithm for 3D edge detection by Yague-Fabra et al[vi]. Since the limits of our sensor's acquisition limit resolution, applying a

frequency-based filter to attenuate image noise is likely to filter some high-frequency signal components that constitute features and not artifacts. Canny is particularly suited for such an application, as the filter is Gaussian. The image is convolved with a 3D discretization of a bell curve. Then, the maximum gradient is computed along each axis of the image. The highest intensity gradients represent edges. To achieve gradient calculation in each direction a convolution mask should be applied in the direction of interest. The output of the gradient calculation is three planes of gradient intensity which show interfacial morphology[vii].

In a normal application of Canny edge detection the planar interfacial morphology information would be filtered to achieve a thinner edge before mapping edge information back to the original image[viii]. However this information is actually acceptable for our uses. Given the three planes of intensity data we can gather data belonging to one cell by simply comparing the coordinates of high intensity gradient at the intersection of planes. Then a linearization of the membrane morphology can be achieved by comparing the displacement of the peak gradient intensities from a sphere of the same volume. This estimation is physiologically relevant since membrane blebbing presents as spherical protrusions from a shrinking spherical cell[ix]. A model that accounts for the volume loss of up to 50% by the main apoptotic cell body[x] may be explored in a later development cycle. For each cell a standard deviation from the sphere will be computed.

The final step in determining apoptotic percentage of cells in sample is to sort the standard deviations with a linear classifier. The classifier should be trained in trials prior to release of software because it will take several trials to fit the data. Since simultaneous measurement of apoptosis on the single cellular level by our system and by a comparative technology is impossible, and there is no way to guarantee against apoptosis induction over time, a cell-by-cell training of the classifier is difficult. Therefore instead, the system will be trained on cells under procedures known to induce apoptosis at certain rates, such as incubation with hydrogen peroxide[xi]. A support vector machine (SVM) is appropriate for this mode of pattern recognition since it is non-probabilistic classifier which learns the separation criteria that generates the greatest possible gap between classes.

The final output of the software is a percentage of apoptotic cells for each sample measured. Error bars will be included to represent at least a 95% confidence interval as determined during testing of the classifier. This

data will be immediately saved down to the hard drive to prevent accidental loss of data by the user, as dictated by the requirements.

---

[i] Bishara, W. et al. "Lensfree on-chip microscopy over a wide field-of-view using pixel super-resolution." *Optics Express* 18.11 (2010): 11181-11191.

[ii] Greenbaum, A. et al. "Increased space-bandwidth product in pixel super-resolved lensfree on-chip microscopy." *Scientific Reports* 3 (2013).

[iii] Dixon, L. "Holographic deconvolution microscopy for high-resolution particle tracking." *Optics Express* 19 (2011): 16410-16417.

[iv] Gorocs, Z. et al. "In-line color digital holographic microscope for water quality measurements." *Laser Applications in Life Sciences* 7376 (2010): 1-10.

[v] Canny, J. "A computational approach to edge detection." *IEEE Translation Pattern Analysis* 8.60 (2010): 679-698.

[vi] Yague-Fabra, J. A. et al. "A 3D edge detection technique for surface extraction in computed tomography for dimensional metrology applications." 62.1 (2013): 531-534.

[vii] Kimmel, R. and A. M. Bruckstein. "Regularized laplacian zero crossings as optimal edge integrators." *International Journal of Computer Vision* 53.3 (2003): 225-243.

[viii] Bao, P. et al. "Canny edge detection enhancement by scale multiplication." *IEEE Transactions on Pattern Analysis and Machine Intelligence* 27.9 (2005): 1485-1490.

[ix] Khmaladze, A. et al. "Digital holographic microscopy study of early morphological changes during apoptosis." *Digital Holography and Three-Dimensional Imaging Conference* (2010).

[x] Kim, K. "AFM-detected apoptotic changes in morphology and biophysical property caused by paclitaxel in Ishikawa and HeLa cells." *PLoS ONE* 7 (2012).

[xi] Cerella, C. et al. "Multiple mechanisms for hydrogen peroxide-induced apoptosis." *Annals of the New York Academy of Science* 1771 (2009): 559-563.